CHALMERS
UNIVERSITY OF TECHNOLOGY

Effects of state of charge on elastic properties of 3D structural battery composites

Citation for the original published paper (version of record):
Carlstedt, D., Marklund, E., Asp, L. (2019). Effects of state of charge on elastic properties of 3D structural battery composites. Composites Science and Technology, 169: 26-33.
http://dx.doi.org/10.1016/j.compscitech.2018.10.033

Accepted Manuscript

Effects of state of charge on elastic properties of 3D structural battery composites

David Carlstedt, Erik Marklund, Leif E. Asp

PII: S0266-3538(18)32088-8

DOI: https://doi.org/10.1016/j.compscitech.2018.10.033

Reference: CSTE 7440

To appear in: *Composites Science and Technology*

Received Date: 28 August 2018

Revised Date: 25 October 2018

Accepted Date: 26 October 2018

Please cite this article as: Carlstedt D, Marklund E, Asp LE, Effects of state of charge on elastic properties of 3D structural battery composites, *Composites Science and Technology* (2018), doi: https://doi.org/10.1016/j.compscitech.2018.10.033.

Effects of state of charge on elastic properties of 3D structural battery composites

David Carlstedt[1], Erik Marklund[2,3], Leif E. Asp[1*]

[1] Department of Industrial and Materials Science, Chalmers University of Technology, SE-412 96 Gothenburg, Sweden

[2] RISE SICOMP AB, SE-431 22 Mölndal, Sweden

[3] Department of Engineering Sciences and Mathematics, Luleå University of Technology, SE-971 87 Luleå, Sweden

∗ Corresponding author. E-mail: leif.asp@chalmers.se

Abstract: The effects of state of charge (SOC) on the elastic properties of 3D structural battery composites are studied. An analytical model based on micromechanical models is developed to estimate the effective elastic properties of 3D structural battery composite laminae at different SOC. A parametric study is performed to evaluate how different design parameters such as volume fraction of active materials, stiffness of constituents, type of positive electrode material, etc. affect the moduli of the composite lamina for extremes in SOC. Critical parameters and configurations resulting in large variations in elastic properties due to change in SOC are identified. As the extreme cases are of primary interest in structural design, the effective elastic properties are only estimated for the electrochemical states corresponding to discharged (SOC=0) and fully charged (SOC=1) battery. The change in SOC is simulated by varying the volume and elastic properties of the constituents based on data from literature. Parametric finite element (FE) models for square and hexagonal fibre packing arrangements are also analysed in the commercial FE software COMSOL and used to validate the analytical model. The present study shows that the transverse elastic properties E_2 and G_{23} and the in-plane shear modulus G_{12} are strongly affected by the SOC while the

longitudinal stiffness E_1 is not. Fibre volume fraction and the properties of the coating (such as stiffness and Poisson's ratio) are identified as critical parameters that have significant impact on the effect of SOC on the effective elastic properties of the composite lamina. For configurations with fibre volume fraction $V_f \geq 0.4$ and Young's modulus of the coating of 1 GPa or higher, the transverse properties E_2 and G_{23} change more than 30% between extremes in SOC. Furthermore, for configurations with high volume fractions of electrode materials and coating properties approaching those of rubber the predicted change in transverse stiffness E_2 is as high as +43%. This shows that it is crucial to take effects of SOC on the elastic properties into account when designing 3D structural battery composite components.

Keywords: A. Carbon fibres; A. Functional composites; B. Electrical properties; C. Elastic properties; C. Modelling

1. Introduction

The structural battery composite is a class of composite materials with ability to store electrical energy in the form of chemical energy (i.e. work as a battery) while simultaneously provide mechanical integrity in a structural system. One promising approach for realising a structural battery is the three-dimensional (3D) battery architecture developed by Asp and co-workers [1–3]. In the 3D structural battery architecture, the carbon fibres work as mechanical reinforcement in a polymer matrix and simultaneously function as negative electrodes in the battery cell. Carbon fibres are used due to their high specific mechanical and electrical properties [4, 5]. The carbon fibres are coated with a thin polymer coating which works as a combined electrolyte and separator layer [6]. The surrounding polymer matrix is doped with lithium-metal-oxide based particles to work as positive electrode in the battery cell. The benefit of using this cell concept is that it significantly reduces the distance between

electrodes and thereby reduce ohmic losses due to the low ion conductivity of the solid polymer electrolyte coating [3]. The 3D battery architecture is illustrated in Fig. 1.

The 3D battery architecture illustrated in Fig. 1 corresponds to a composite lamina. When applied in a structural system several of these battery laminae will be stacked in different configurations, as done in ordinary composite laminates. As the battery composite laminae are electrically conductive they need to be insulated from neighbouring plies. Furthermore, the structural battery composite is sensitive to moisture and must be protected from exposure to moist. This can be done by adding a coating layer or pouch cell materials on the outer surfaces of the components and adding connection points for the current collectors. Some of these practical issues and additional discussions on the application of the structural battery composites in load carrying structures have been presented by Asp and Greenhalgh [7].

It is well known that battery electrodes expand/shrink due to insertion/exit of lithium ions in the electrode materials (i.e. charging/discharging of the battery). Jacques et al. [8] showed that insertion of lithium ions into carbon fibres causes the fibre to expand approximately 1% in longitudinal direction and 8-13% in radial direction. It is also known that positive electrode materials undergo significant volume changes. For example, Mn_2O_4 particles expand/shrink approximately 7% due to lithiation/delithiation [9]. In addition to the volume change it has also been shown that the elastic properties of battery electrode materials such as carbon fibres, graphite and positive electrode particles are affected by lithium-ion concentration [9–12]. The variation of the volume expansion/shrinkage and lithium concentration in the electrode materials are directly linked to the state of charge (SOC) of the battery, which refers to the amount of energy currently stored in the battery.

As the electrochemically active materials (i.e. the electrodes) in ordinary lithium-ion batteries are not designed to carry load, effects of state of charge on mechanical integrity are mainly considered from a safety and durability point of view, e.g. to avoid short circuit or damage to

the electrodes [13–15]. Jun Xu et al. [15], investigated electrochemical failure behaviour for traditional lithium-ion batteries with various SOC and noticed that the mechanical behaviour of the battery electrodes is highly dependent on SOC. The experimental results showed that the structural stiffness increased for higher SOC. In the work by Johannisson et al. [16] results also suggest that the elastic properties of laminated structural battery half-cells change due to change in SOC. The experimental results presented by Johannisson and co-workers indicate an increase in the transverse stiffness of the UD composite lamina (i.e. negative half-cell) of approximately 10% when charged compared to virgin state. Existing work, which deals with computational modelling of structural batteries, focus on modelling the coupling between mechanical and electrochemical response to predict displacements and stresses induced by electrochemical cycling. Pupurs et al. [17] studied how the internal stresses in carbon fibres are affected by lithium concentration gradients associated with electrochemical cycling. Johanna Xu et al. [18, 19] developed a framework in COMSOL for multiphysics modelling of the 3D structural battery to predict internal stresses due to swelling/shrinkage of the constituents related to the electrochemical reactions. Furthermore, an analytical model to predict the deformations and stresses in laminated structural batteries has been developed by Dionisi et al. [20]. In contrast to ordinary batteries, the active materials in the structural battery are intended to carry mechanical load. Consequently, it is crucial to understand and be able to predict any change in the elastic properties of the composite with change in SOC when evaluating the structural performance of the material. To date a model to predict effects of electrochemical cycling on the constitutive properties of a 3D structural battery is lacking.

In this paper an analytical model based on available micromechanical models is developed to investigate how the elastic properties of the 3D structural battery composite are affected by changes in volume and stiffness of constituents associated with a change in SOC. A parametric study is performed using the developed model to analyse how different design

parameters such as volume fraction of active materials, stiffness of constituents, type of positive electrode material, etc. affect the moduli of the structural battery composite for extremes in SOC. The effective elastic properties of the composite lamina are estimated for a discharged (SOC=0) and fully charged (SOC=1) battery and critical parameters / configurations resulting in large changes in elastic properties due to change in SOC are identified. The developed analytical model is based on the Composite Spheres Assemblage (CSA) model presented by Hashin [21] and a generalisation of the Composite Cylinder Assemblage (CCA) [21–23] for N-phase composites expressed by Marklund et al. [24], here referred to as N-phase CCA. The CSA model and the N-phase CCA model are combined and used to estimate the effective elastic properties of the lamina for different SOC. The change in SOC is simulated by varying the volume and elastic properties of the constituents based on data from literature. To validate the analytical model parametric finite element (FE) models for square and hexagonal fibre packing arrangements are developed in the commercial FE software COMSOL. The FE models are used to estimate the effective elastic properties of the composite lamina for the two packing arrangements and the results are compared with the results from the analytical model.

It should be noted that stress distributions are not reported in this work. The reason is that it is unlikely that the two electrochemical steady states generate the most severe stress states. That is, concentrations gradients in constituents, thermal effect, etc., which further depend on charge/discharge rate are currently not considered. This will affect the stresses at the microlevel during electrochemical cycling.

2. Materials and geometry

The 3D structural battery cell consists of three phases: the carbon fibre that acts as the negative electrode, the polymer coating that acts as combined electrolyte and separator and finally the particle reinforced matrix that acts as the positive electrode (Fig. 2). The

electrochemically active materials on the negative side of the battery are carbon fibres and on the positive side lithium-metal-oxide based particles distributed within the polymer matrix. In addition, the matrix is doped with carbon black to conduct electrons.

The carbon fibres are assumed to be IMS65 unsized fibres and the coating is assumed to be made of the polymer system developed by Leijonmark et al. [6]. The elastic properties for this polymer system can be altered by changing the cross-linking density in relation to the ethylene oxide groups as described in the study by Leijonmark. The positive electrode matrix is assumed to be made of a bi-continuous polymer network developed by Ihrner et al. [25]. The elastic properties of this system have been studied by Ihrner and co-workers and as described by the authors the elastic properties of this polymer system can be altered by changing the chemical composition. The polymer matrix is reinforced with lithium metal particles used in commercially available batteries.

2.1 Effects of state of charge on volume and stiffness of constituents

Volume and stiffness changes of battery electrode materials have been reported in [8–12] and values for the electrode materials considered in this study are summarized in Table 1. The volume and stiffness changes are stated as the change in volume and stiffness of the constituents moving from the delithiated state of the material (i.e. when it does not contain any lithium-ions) to the lithiated state. It should be noted that the change in longitudinal stiffness of carbon fibres is negative and is defined with respect to the ratio between the fibre volume fraction in delithiated state $V_{\mathrm{f},dl}$ and the fibre volume fraction in lithiated state $V_{\mathrm{f},l}$. This assumption is based on measurements by Jacques et al. [10] who showed that the nominal longitudinal stiffness was unaffected by the lithiation degree while the cross-section area of the fibre increased approximately 10%. This means that the axial elastic modulus must decrease in proportion to the increase in cross-section area. The change in transverse stiffness of carbon fibres due to lithiation is to the authors knowledge unknown. However, a

change in stiffness of graphite used in commercially available Li-ion batteries have been reported by Qi et al. [11]. In that study, it was seen that the out-of-basal-plane stiffness increase approximately 150% while the in-basal-plane stiffness components decreased slightly as the graphite was lithiated. We assume the graphite planes within the carbon fibre to be mainly arranged along the fibre direction. Thus, the change in transverse stiffness for the carbon fibre is expected to be similar to the change in out-of-basal-plane stiffness of graphite. It should also be noted that the positive electrode particles are modelled as isotropic, homogeneous particles. Hence, average elastic modulus of the particles, E_{p}, is used in the analysis.

3. Analytical model

The developed analytical model used to estimate the effective elastic properties of the 3D structural battery composite at different SOC is set-up in four steps. In step 1 the elastic properties and volume fractions of the constituents are updated based on input data for the given SOC. In step 2 the CSA model is used to calculate the effective elastic properties of the particle reinforced matrix (the positive electrode). In step 3 the N-phase CCA model is used to compute the effective elastic properties of the three-phase system (fibre, coating and particle reinforced matrix) using the effective elastic properties of the particle reinforced matrix from step 2 as input. In a final step the change in elastic properties between the evaluated SOC is calculated. Details of step 1-3 are given below.

3.1 Effects of state of charge on moduli and volume fractions (step 1)

With respect to structural design the extreme cases are critical and for this reason only the electrochemical states corresponding to discharged (SOC=0) and fully charged (SOC=1) battery are considered. In the fully charged state the carbon fibres are assumed to be fully lithiated and the positive electrode particles are assumed to be delithiated. In the discharged state the opposite conditions are assumed. The electrochemical states are assumed to be

frozen, i.e. the electrochemical reactions are assumed to be unaffected by the applied mechanical load within the frame of reference (small deformations), as shown for carbon fibres by Jacques et al. [10]. The material response is assumed to be linear elastic. The changes in elastic properties are applied by changing the properties of the constituents for the given SOC. The stiffness of the active materials (fibres and particles) are defined as

$$E_{\mathrm{f}}^{\mathrm{L}} = E_{\mathrm{f},dl}^{\mathrm{L}}\left(1 + \mathrm{SOC}\cdot\Delta E_{\mathrm{f}}^{\mathrm{L}}\right),\ E_{\mathrm{f}}^{\mathrm{T}} = E_{\mathrm{f},dl}^{\mathrm{T}}\left(1 + \mathrm{SOC}\cdot\Delta E_{\mathrm{f}}^{\mathrm{T}}\right),\ G_{\mathrm{f}}^{\mathrm{TT}} = \frac{E_{\mathrm{f}}^{\mathrm{T}}}{2\left(1+\nu_{\mathrm{f}}^{\mathrm{TT}}\right)}, \quad (1)$$

$$E_{\mathrm{p}} = E_{\mathrm{p},dl}\left(1 + (1 - \mathrm{SOC})\cdot\Delta E_{\mathrm{p}}\right), \quad (2)$$

where $E_{\mathrm{f}}^{\mathrm{L}}$, $E_{\mathrm{f}}^{\mathrm{T}}$ and $G_{\mathrm{f}}^{\mathrm{TT}}$ are the longitudinal, transverse and transverse shear moduli of the carbon fibres (subscript f) and E_{p} is Young's modulus of the positive electrode particles (subscript p). The moduli of the constituents in the delithiated state (subscript *dl*) are denoted as $E_{\mathrm{f},dl}^{\mathrm{L}}$, $E_{\mathrm{f},dl}^{\mathrm{T}}$ and $E_{\mathrm{p},dl}$ respectively. In Eqs. (1) and (2) the state of charge is defined as SOC, which is equal to one for fully charged state and equal to zero for discharged state. The changes in stiffness $\Delta E_{\mathrm{f}}^{\mathrm{L}}$, $\Delta E_{\mathrm{f}}^{\mathrm{T}}$ and ΔE_{p} are defined as the expected change going from delithiated to lithiated state and are given in Table 1. As the stiffness of the coating and matrix are significantly lower than the transverse stiffness of the carbon fibres and the stiffness of the particles, the volume changes of the active materials are assumed to be unconstrained. The volume of the non-active materials is assumed to be constant and the outer surface of the composite free to expand. Hence, the volume fractions need to be updated/normalized with respect to the total change in volume of the cross section for each SOC different from the neutral state, i.e. the state in which the composite is manufactured. In this analysis the discharged state (SOC=0) is defined as the neutral state in which the fibres are delithiated $V_{\mathrm{f},dl}$ and the positive electrode particles are lithiated $V_{\mathrm{p},l}$. The sum of the volume fractions of the constituents for the neutral state is therefore defined as

$$V_{\mathrm{f},dl} + V_{\mathrm{c}} + V_{\mathrm{m}} + V_{\mathrm{p},l} = 1. \quad (3)$$

In Eq. (3) V_{c} and V_{m} are volume fractions of coating (subscript c) and matrix (subscript m) respectively. In the fully charged state (SOC=1) the volume fractions of the active electrode constituents, i.e. fibres and particles, are updated according to the volume changes presented in Table 1. In this state the fibres are lithiated $V_{\mathrm{f},l}$ and the positive electrode particles are delithiated $V_{\mathrm{p},dl}$. The sum of volume fractions, after applying the changes of the volume fractions of fibres ΔV_{f} and particles ΔV_{p}, is defined as

$$\sum V = V_{\mathrm{f},dl}(1 + \Delta V_{\mathrm{f}}) + V_{\mathrm{c}} + V_{\mathrm{m}} + V_{\mathrm{p},l}\left(1 - \Delta V_{\mathrm{p}}\right). \quad (4)$$

The volume changes of the active materials are assumed to be unconstrained and the volume of the non-active materials is assumed to be constant. This means that the sum of volume fractions in Eq. (4) does not have to be equal to one. The volume fractions of the constituents in the charged state are therefore normalized with respect to the total volume fraction from Eq. (4). The sum of normalized volume fractions is expressed as

$$\frac{V_{\mathrm{f},dl}(1+\Delta V_{\mathrm{f}})+V_{\mathrm{c}}+V_{\mathrm{m}}+V_{\mathrm{p},l}(1-\Delta V_{\mathrm{p}})}{\sum V} = V_{\mathrm{f},l} + \frac{V_{\mathrm{c}}}{\sum V} + \frac{V_{\mathrm{m}}}{\sum V} + V_{\mathrm{p},dl} = 1. \quad (5)$$

3.2 Micromechanical models (step 2 and 3)

In the second step of the analytical model the effective properties of the particle reinforced matrix are calculated using the CSA model developed by Hashin [21]. The effective Young's modulus is given by

$$E_{\mathrm{m}}^{\mathrm{eff}} = \frac{9K^{\mathrm{eff}}G^{\mathrm{eff}}}{3K^{\mathrm{eff}}+G^{\mathrm{eff}}}, \quad (6)$$

where the effective bulk modulus K^{eff} is defined as

$$K^{\mathrm{eff}} = K_{\mathrm{m}} + \frac{(K_{\mathrm{p}}-K_{\mathrm{m}})(3K_{\mathrm{m}}+4G_{\mathrm{m}})V_{\mathrm{p}}^{*}}{3K_{\mathrm{p}}+4G_{\mathrm{m}}-3(K_{\mathrm{p}}-K_{\mathrm{m}})V_{\mathrm{p}}^{*}}. \quad (7)$$

The subscripts m and p in Eq. (7) denotes matrix and particle properties respectively and V_{p}^{*} is the volume fraction of particles within the matrix (not to be confused with V_{p} defined as $V_{\mathrm{p}} = V_{\mathrm{p}}^{*}V_{\mathrm{m}}$). The effective shear modulus G^{eff} is calculated solving the quadratic equation

$$A\left(\frac{G^{\mathrm{eff}}}{G_{\mathrm{m}}}\right)^{2} + 2B\left(\frac{G^{\mathrm{eff}}}{G_{\mathrm{m}}}\right) + C = 0. \tag{8}$$

The constants A, B and C in Eq. (8) are calculated based on the shear modulus and Poisson's ratio of the two phases as described in [26]. This method is referred to as the generalized self-consistent method [23, 26]. It should be noted that the stiffness of the particles E_{p} and the volume fraction of particles within the matrix V_{p}^{*} are updated for each SOC.

In the third step of the analytical model the effective elastic properties of the three-phase system (fibre, coating and particle reinforced matrix) are estimated using the N-phase CCA model developed by Marklund et al. [24]. The cylinder representation of the three-phase system used in the N-phase CCA model is illustrated in Fig. 3. The effective properties of the homogenised particle reinforced matrix derived in step 2 are used as input for the properties of the particle reinforced matrix. The transverse bulk modulus of the three-phase system K_{23} is given as

$$K_{23} = \frac{A_1^N \beta_N r_N^{\alpha_N - 1} + A_2^N \gamma_N r_N^{-\alpha_N - 1}}{2\varepsilon_0}, \tag{9}$$

where r_N corresponds to radius of the outer cylinder surface and β_N, γ_N and α_N are functions of the *N*-th phase's elastic constants given in [24]. The unknown constants A_1^N, A_2^N are derived by solving the micromechanics stress problem for nonzero uniform strain ε_0 in the radial and hoop directions under the assumption of transverse plane strain. In the case of a three-phase system *N* is equal to three. The longitudinal modulus E_1 and Poisson's ratio v_{12} are derived as

$$E_1 = \frac{2}{\varepsilon_{10} r_N^2}\left(\varepsilon_{10}\sum_{k=1}^{N}\frac{g_k\left(r_k^2 - r_{k-1}^2\right)}{2} + \sum_{k=1}^{N}\frac{A_1^k f_k\left(r_k^{\alpha_k+1} - r_{k-1}^{\alpha_k+1}\right)}{\alpha_k+1} + \sum_{k=2}^{N}\frac{A_2^k h_k\left(r_k^{-\alpha_k+1} - r_{k-1}^{-\alpha_k+1}\right)}{-\alpha_k+1}\right), \quad (10)$$

$$v_{12} = \frac{-\psi_N\varepsilon_{10} - A_1^N r_N^{\alpha_N-1} - A_2^N r_N^{-\alpha_N-1}}{\varepsilon_{10}}. \quad (11)$$

In Eqs. (10) and (11) r_k is the radius of the *k*-th cylinder and α_k, ψ_k, g_k, f_k and h_k are functions of the *k*-th phase's elastic constants given in [24]. The unknown constants A_1^k, A_2^k are calculated by solving the micromechanics stress problem for nonzero uniform strain ε_{10} in the longitudinal direction assuming free contraction in the radial direction. The in-plane shear modulus G_{12} is calculated as

$$G_{12} = \frac{G_{1r}^N\left(A_1^N\alpha_N r_N^{\alpha_N-1} - A_2^N\alpha_N r_N^{-\alpha_N-1}\right)}{\gamma_{12}^0}, \quad (12)$$

where the unknown constants A_1^N, A_2^N in Eq. (12) are calculated solving the micromechanics stress problem for nonzero pure in-plane shear strain γ_{12}^0. The transverse shear modulus G_{23} is calculated solving the micromechanics stress problem under pure shear loading in the transverse plane. Displacement and stress continuity conditions are defined and set-up in a system of equations. The system of equations is solved by iterative reduction of a misfit function for stress continuity at the composite interface. The transverse stiffness E_2 and Poisson's ratio v_{23} is calculated based on the derived elastic constants K_{23} and G_{23}, given as

$$E_2 = \frac{1}{\left(\frac{1}{4K_{23}} + \frac{1}{4G_{23}} + \frac{v_{12}^2}{E_1}\right)}, \text{ and} \quad (13)$$

$$v_{23} = \frac{E_2}{2G_{23}} - 1. \quad (14)$$

Detailed derivation and step-by-step procedure for implementing the N-phase CCA model are given by Marklund et al. [24]. The elastic properties of the three phases (fibre, coating and particle reinforced matrix) and the radius of the individual cylinders (related to volume fractions) are updated for each SOC as described in section 3.1.

4. Computational models

The computational models are set-up in the commercial FE software *COMSOL 5.3* and the numerical homogenisation is prepared in accordance to the procedure described by Barbero [27]. Two parametric FE models for square and hexagonal fibre packing arrangements are analysed. The models are repeatable unit cells (RUCs) and are used to predict the effective elastic properties of the composite lamina for the two arrangements. The FE models are 3D models using 20 node solid elements with three degrees of freedom at each node and orthotropic material properties are assumed. Input values for the volume fractions, stiffness of constituents, etc. are defined as parametric variables in the FE models, which makes it possible to vary the input values by running parametric sweeps. The elastic properties and volume fractions of the constituents are updated as described in Section 3.1. The results from the FE models are used to validate the analytical model.

5. Parametric study

A series of material and geometrical properties have been collected from various studies. The variables, including range studied, evaluated in the parametric study are presented in Table 2. The baseline values are referred to as the baseline configuration. Based on experimental data [6, 25, 28] the Young's modulus of the coating and matrix are assumed to be 0.1 GPa and 0.5 GPa respectively for the baseline case. The matrix is also reinforced with lithium metal particles which further enhance the effective stiffness of the particle reinforced matrix (for the baseline case in discharged state $E_{\mathrm{m}}^{\mathrm{eff}}$ = 1.81 GPa). For most configurations considered in the parametric study the stiffness of the coating will therefore be lower than the particle

reinforced matrix due to the difference in assumed elastic properties and the reinforcing effect of the particles in the matrix.

The parametric study is performed varying the parameters individually within the specified range, while the remaining parameters are kept constant at their baseline value reported in Table 2. The studied range of the coating and matrix properties are based on assumed variability of the polymer systems linked to change in compositions as described in the respective studies. In the parametric study the densities of the coating and the polymer matrix are assumed constant, while their elastic properties are varied. This assumption has minor effect on the electrical performance (which depend on the density of the constituents).

6. Results and discussion

The results from the parametric study are summarised below. The complete collection of results is available in Supplementary data.

6.1 Baseline

The effective elastic properties for the baseline configuration are calculated for SOC=0 and SOC=1 using the developed analytical model, and the FE models for validation. The results are presented in Table 3. For the baseline configuration the longitudinal stiffness E_1 and the in-plane shear stiffness G_{12} decreases by -0.1% and -0.8% respectively when the battery is charged (SOC=1) compared to when discharged (SOC=0), while the transverse properties E_2 and G_{23} increases approximately +3%. This is due to the fact of that the nominal stiffness of the carbon fibres in the longitudinal direction does not change with SOC. The small reduction in the longitudinal stiffness E_1 is a result of changes in the properties of the positive electrode particles resulting in decreased effective stiffness of the particle reinforced matrix. The change in the remaining properties are mainly caused by changes in cross-section and

transverse stiffness of the carbon fibres. The results also show very good agreement between the analytical results and the numerical predictions.

6.2 Influence of negative electrode properties

To study the influence of the fibre volume fraction on the effect of SOC on the elastic properties of the composite lamina the effective elastic properties are calculated varying the fibre volume fraction from 0.2-0.6 as shown in Fig. 4. For high volume fractions (V_f > 0.5), the difference between charged and discharged state for the elastic properties E_2, G_{12} and G_{23} are in the range of 5-10%. For V_f = 0.6 the transverse stiffness E_2 is approximately 8% higher in charged state compared to when discharged. The state of charge has minor effect on the longitudinal stiffness E_1. It should also be noted that the transverse stiffness E_2 decreases with increasing fibre volume fraction. This effect is a result of the relative increase of the volume fraction of the soft coating with increased fibre volume fraction as the thickness of the coating is constant for every choice of V_f. In Fig. 4 it can also be observed that the predicted results from the analytical model shows very good agreement with the results from the FE models for all evaluated fibre volume fractions. The transverse modulus of the carbon fibre E_f^T and the change in transverse modulus with change in SOC $\Delta E_\mathrm{f}^\mathrm{T}$ are also varied within the ranges given in Table 2 and the complete results are presented in Supplementary data. In the case of no change in transverse stiffness of the carbon fibre ($\Delta E_\mathrm{f}^\mathrm{T}$ = 0%), the change in the transverse stiffness E_2 with change in SOC is only +0.2% for the baseline (V_f = 0.4) but still +4% for V_f = 0.6 (to be compared with +3% and +8% respectively in case of $\Delta E_\mathrm{f}^\mathrm{T}$ = 150%). In the case of increased transverse stiffness of the fibre (E_f^T = 25 GPa) the change in the transverse stiffness E_2 is +1.7% for the baseline (V_f = 0.4) and +6% for V_f = 0.6. For a stiffer surrounding medium, the influence of transverse properties of the fibre on the effect of SOC on the elastic properties are enhanced. The influence of the transverse properties of the fibres on the effect of SOC on the elastic properties of the composite is

found to depend on the stiffness ratios $E_{\mathrm{f}}^{\mathrm{T}}/E_{\mathrm{c}}$ and $E_{\mathrm{f}}^{\mathrm{T}}/E_{\mathrm{m}}^{\mathrm{eff}}$. These results show that the effect of SOC on transverse elastic properties E_2 and G_{23} are highly influenced by the fibre volume fraction and assumed transverse properties of the carbon fibres.

6.3 Influence of solid polymer electrolyte coating properties

In this section the influence of the properties of the coating on the effective elastic properties of the composite lamina for different SOC is studied by varying the stiffness, Poisson's ratio and thickness of the coating. Figure 5 shows the transverse stiffness E_2 and in-plane shear stiffness G_{12} at SOC=0 and SOC=1 varying Young's modulus of the polymer coating from 1 MPa to 3 GPa. It is clear that the stiffness of the coating has a significant effect on the transverse and shear stiffness of the composite. Moreover, these stiffnesses are strongly affected by the state of charge. From Fig. 5, it can be observed that for the baseline case (E_{c} = 0.1 GPa) the change in the transverse stiffness E_2 with change in SOC is only +3% which is significantly lower compared with the cases of very soft coating (E_{c} = 1 MPa) and stiff coating (E_{c} = 3 GPa) with changes of -16% and +20% respectively. Also, the change of the in-plane shear stiffness G_{12} is only -1% for the baseline case while -10% and +10% for E_{c} = 1 MPa and E_{c} = 3 GPa, respectively. For a fibre volume fraction of 0.6 and a Young's modulus of the coating of 1 GPa the change in transverse stiffness E_2 is predicted to be as high as +30% as the battery is charged (3.5 GPa at SOC=0 vs. 4.6 GPa at SOC=1). It should be noted that the properties of the coating have only minor effect on the longitudinal stiffness E_1 (less than -0.1% change within the studied range).

Poisson's ratio of the coating has significant impact on the effect of SOC on the effective transverse elastic properties E_2 and G_{23} of the composite as shown in Fig. 6. For high values of Poisson's ratio close to 0.5 (similar to rubber), the difference with SOC is +14% for the baseline case, while it is only +1% for a Poisson's ratio of 0.2. For a configuration of V_{f} = 0.6

and E_c = 1 GPa and with a Poisson's ratio of the coating of 0.45 (close to rubber) the difference between extremes is as high as 37%. This shows that the properties of the coating are crucial for the stiffness of the composite lamina as well as for stiffness consistency with SOC. Furthermore, effects of coating thickness highly depend on its constitutive properties. Therefore, no general conclusions on how coating thickness influence the lamina properties can be drawn.

6.4 Influence of positive electrode properties

The influence of the properties of the positive electrode (particle reinforced matrix) on the effect of SOC on the effective elastic properties of the composite lamina are studied by varying the type of electrode particles, stiffness of the polymer matrix and volume fraction of particles. The effect of SOC on the elastic properties is studied for three different electrode materials (given in Table 2). The change in stiffness between SOC=0 and SOC=1 is largest for $LiCoO_2$ due to the fact that the stiffness of the CoO_2 particles increases approximately 350% when lithiated [9]. For the baseline configuration the change in transverse stiffness E_2 is +5.6% for $LiCoO_2$ while only +2% for $LiMn_2O_4$ and +3% for $LiFePO_4$. For configurations with higher stiffness of the surrounding matrix and higher volume fraction of particles, this effect is enhanced. Consequently, for configurations with high concentrations of $LiCoO_2$ in a stiff polymer matrix, large change in effective elastic properties due to change in SOC can be expected. In the case of V_f = 0.6, $E_m = E_c$ = 1 GPa, ν_c = 0.45 and V_p^* = 0.6 of $LiCoO_2$ in the matrix the change in transverse stiffness between SOC=0 and SOC=1 is approximately +43%. It should be noted that the choice of positive electrode material and the volume fraction of active materials (fibres and particles) also have significant impact on the electrical performance. Predicted specific capacities for the studied configurations are presented in Supplementary data.

6.5 Effects on laminate level

The effects from changes in elastic properties of the unidirectional lamina are compared with the effects of SOC on the elastic properties of a $[0/90]_S$ laminate. For this laminate configuration the changes of the transverse elastic property of the individual laminae are suppressed for the elastic properties of the laminate in the 0 and 90-degree directions. On the other hand, the in-plane shear stiffness of the laminate is highly affected by SOC. For the critical configuration described in previous section with a predicted change in transverse stiffness of the individual laminae of approximately +43% the change in in-plane shear stiffness of the laminate is approximately +40%. The change in in-plane elastic properties in the 0 and 90-degree directions is only about +1%. This provides additional information regarding the effects of SOC at a laminate level.

Changes in moduli of the individual laminae will also affect the macroscopic stress distribution in the composite laminate. A significant increase in the transverse stiffness of the laminae, while the longitudinal stiffness remains nearly constant, will result in redistributed stresses in the laminate potentially leading to earlier crack initiation in the laminae with fibres transverse to the loading direction.

7. Conclusions

In this study, the effects of state of charge (SOC) on the elastic properties of 3D structural batteries are studied. An analytical model based on micromechanical models is developed to estimate the effective elastic properties of a three-phase (carbon fibre, coating and particle reinforced matrix) 3D structural battery composite at different SOC. A parametric study is performed to investigate how design parameters such as volume fraction of active materials, stiffness of constituents, type of positive electrode material, etc. affect the elastic properties of the structural battery composite at different SOC. To validate the analytical model parametric FE models for square and hexagonal fibre packing arrangements were developed

and the results show good agreement between the analytical results and the numerical predictions.

The transverse elastic properties E_2 and G_{23} and the in-plane shear modulus G_{12} are found to be highly affected by the SOC for critical configurations, while the longitudinal stiffness E_1 is not significantly affected by the SOC. Fibre volume fraction and properties of the coating (stiffness and Poisson's ratio) are identified as critical design parameters and have significant impact on the effect of SOC on the elastic properties of the composite lamina. For configurations with a high fibre volume fraction ($V_\mathrm{f} \geq 0.6$) and Young's modulus of the solid polymer electrolyte coating of 1 GPa or higher up to 30% change in transverse stiffness E_2 with a change in SOC is found. In the case of rubbery coating (v_c = 0.45) and high volume fraction of $LiCoO_2$ particles in a stiff polymer matrix ($E_\mathrm{m} = E_\mathrm{c}$ = 1 GPa and $V_\mathrm{p}^* = 0.6$) the predicted change in transverse stiffness E_2 is as high as +43%. This shows that the effects of SOC on the elastic properties are crucial to account for when designing 3D structural battery composite components. Especially in applications where stiffness consistency with SOC is important.

Acknowledgements

This project has been funded by the European Union, Clean Sky Joint Undertaking 2, Horizon 2020 under Grant Agreement Number 738085 and USAF, contract FA9550-17-1-0338, which are gratefully acknowledged.

References

[1] L.E. Asp, A. Bismarck, T. Carlson, G. Lindbergh, S. Leijonmarck, M. Kjell, A battery half-cell, a battery and their manufacture (structural battery). PCT, Patent No. 2893582, November 16th 2016. (Intl Appl No. PCT/EP2013/068024, 2013).

[2] T. Carlson, Multifunctional composite materials – design, manufacture and

experimental characterisation, Doctoral Thesis, Luleå University of Technology, Sweden, 2013.

[3] L.E. Asp, E.S. Greenhalgh, Structural power composites, Compos. Sci. Technol. 101 (2014) 41–61.

[4] G. Fredi, et al., Graphitic microstructure and performance of carbon fibre Li-ion structural battery electrodes, Accepted for publication in Multifunctional Materials.

[5] M.H. Kjell, E. Jacques, D. Zenkert, M. Behm, G. Lindbergh, PAN-based carbon fiber negative electrodes for structural lithium-ion batteries, J. Electrochem. Soc. 158 (2011) A1455–A1460.

[6] S. Leijonmarck, T. Carlson, G. Lindbergh, L.E. Asp, H. Maples, A. Bismarck, Solid polymer electrolyte-coated carbon fibres for structural and novel micro batteries, Compos. Sci. Technol. 89 (2013) 149–157.

[7] L.E. Asp, E.S. Greenhalgh, Chapter 20 – Multifunctional structural battery and supercapacitor composites, Multifunctionality of Polymer Composites, Eds. K. Friedrich and U. Breuer, Elsevier, Oxford, 2015.

[8] E. Jacques, M.H. Kjell, D. Zenkert, G. Lindbergh, M. Behm, Expansion of carbon fibres induced by lithium intercalation for structural electrode applications, Carbon 59 (2013) 246–254.

[9] Y. Qi, L.G. Hector, C. James, K.J. Kim, Lithium Concentration Dependent Elastic Properties of Battery Electrode Materials from First Principles Calculations, J. Electrochem. Soc. 161 (2014) F3010–F3018.

[10] E. Jacques, M.H. Kjell, D. Zenkert, G. Lindbergh, The effect of lithium-intercalation on the mechanical properties of carbon fibres, Carbon 68 (2014) 725–733.

[11] Y. Qi, H. Guo, L.G. Hector, A. Timmons, Threefold Increase in the Young's Modulus of Graphite Negative Electrode during Lithium Intercalation, J. Electrochem. Soc. 157

(2010) A558–A566.

[12] T. Maxisch, G. Ceder, Elastic properties of olivine Lix FePO4 from first principles, Phys. Rev. B - Condens. Matter Mater. Phys. 73 (2006) 1–4.

[13] J. Cannarella, C.B. Arnold, State of health and charge measurements in lithium-ion batteries using mechanical stress, J. Power Sources. 269 (2014) 7–14.

[14] E. Sahraei, J. Campbell, T. Wierzbicki, Modeling and short circuit detection of 18650 Li-ion cells under mechanical abuse conditions, J. Power Sources. 220 (2012) 360–372.

[15] J. Xu, B. Liu, D. Hu, State of Charge Dependent Mechanical Integrity Behavior of 18650 Lithium-ion Batteries, Sci. Rep. 6 (2016) 1–11.

[16] W. Johannisson, N. Ihrner, D. Zenkert, M. Johansson, D. Carlstedt, L.E. Asp, Multifunctional properties of a carbon fiber UD lamina structural battery electrode, Compos. Sci. Technol. 168 (2018) 81-87.

[17] A. Pupurs, J. Varna, Modeling mechanical stress and exfoliation damage in carbon fiber electrodes subjected to cyclic intercalation/deintercalation of lithium ions, Compos. Part B Eng. 65 (2014) 69–79.

[18] J. Xu, G. Lindbergh, J. Varna, Carbon fiber composites with battery function: Stresses and dimensional changes due to Li-ion diffusion, J. Compos. Mater. 52 (2018) 2729–2742.

[19] J. Xu, G. Lindbergh, J. Varna, Multiphysics modeling of mechanical and electrochemical phenomena in structural composites for energy storage: Single carbon fiber micro-battery, J. Reinf. Plast. Compos. 37 (2018) 701–715.

[20] F. Dionisi, R. Harnden, D. Zenkert, A model to analyse deformations and stresses in structural batteries due to electrode expansions, Compos. Struct. 179 (2017) 580–589.

[21] Z. Hashin, Analysis of Composite Materials, J. Appl. Mech. 50 (1983) 481–505.

[22] Z. Hashin, B.W. Rosen, The Elastic Moduli of Fiber-Reinforced Materials, J. Appl. Mech. 31 (1964) 223–232.

[23] R.M. Christensen, K.H. Lo, Solutions for Effective Shear Properties in Three Phase Sphere and Cylinder Models, J. Mech. Phys. Solids. 27 (1979) 315–330.

[24] E. Marklund, J. Varna, R.C. Neagu, E.K. Gamstedt, Stiffness of aligned wood fiber composites: Effect of microstructure and phase properties, J. Compos. Mater. 42 (2008) 2377–2405.

[25] N. Ihrner, W. Johannisson, F. Sieland, D. Zenkert, M. Johansson, Structural Lithium Ion Battery Electrolytes via Reaction Induced Phase-Separation, J. Mater. Chem. A. 5 (2017) 25652–25659.

[26] R.M. Christensen, Mechanics of Composite Materials, Dover publications, Mineola, New York, 2005.

[27] E.J. Barbero, Finite element analysis of composite materials using Ansys, second ed., CRC Press, 2013.

[28] M. Willgert, M.H. Kjell, E. Jacques, M. Behm, G. Lindbergh, M. Johansson, Photoinduced free radical polymerization of thermoset lithium battery electrolytes, Eur. Polym. J. 47 (2011) 2372–2378.

[29] H. Miyagawa, C. Sato, T. Mase, E. Drown, L.T. Drzal, K. Ikegami, Transverse elastic modulus of carbon fibers measured by Raman spectroscopy, Mater. Sci. Eng. A. 412 (2005) 88–92.

Figures

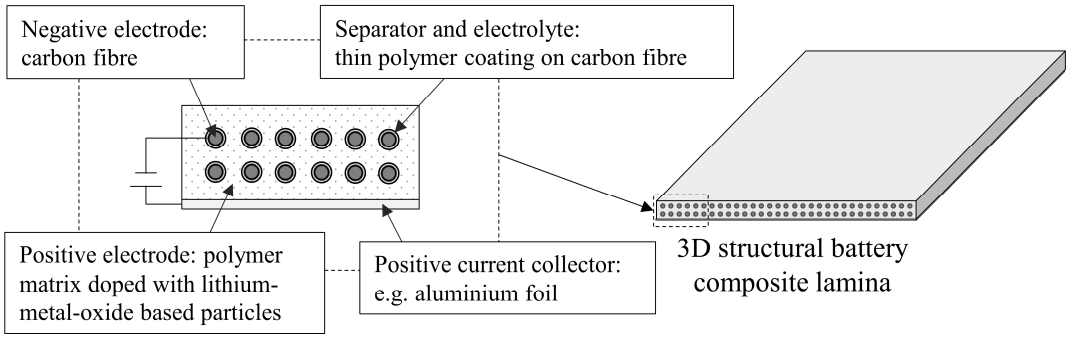

Fig. 1. Schematic illustration of the 3D structural battery composite architecture.

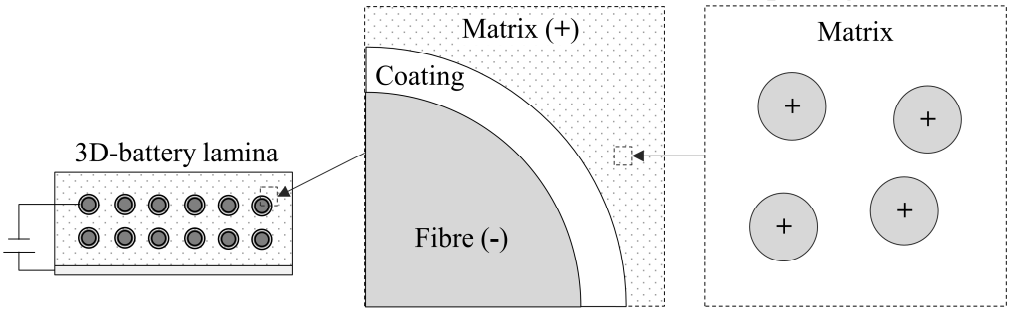

Fig. 2. Illustration of the geometry of the 3D structural battery cell.

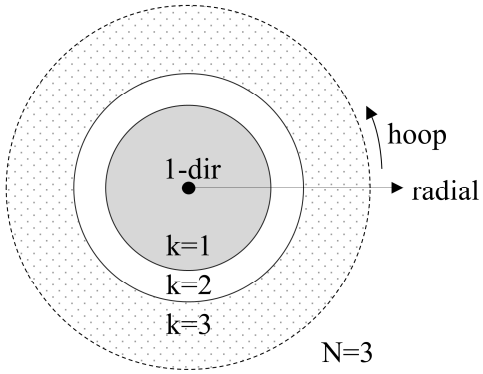

Fig. 3. Cylinder representation of the three-phase system used in the N-phase CCA model (phase 1 fibre, phase 2 coating and phase 3 particle reinforced matrix).

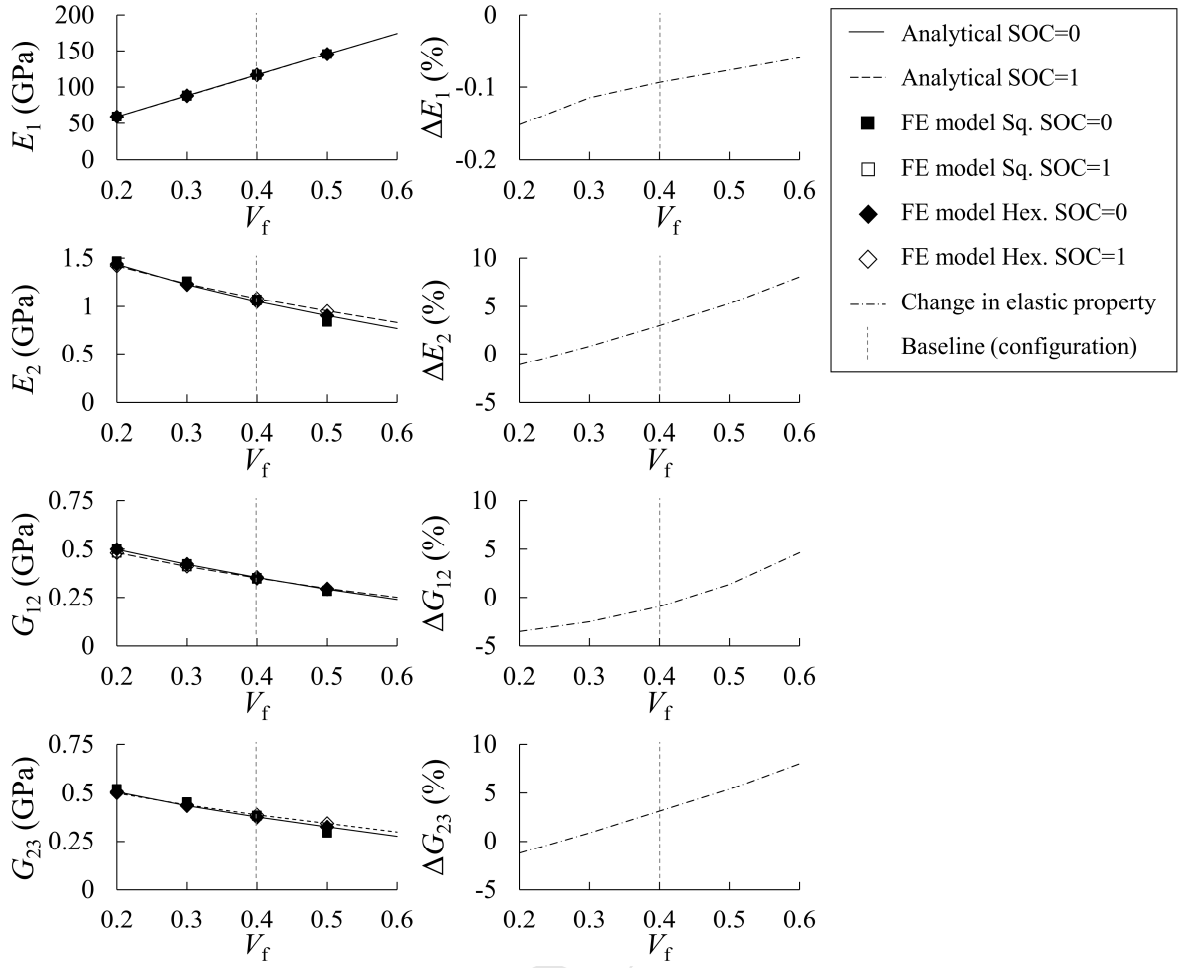

Fig. 4. Variation of effective elastic properties of the composite lamina at SOC=0 and SOC=1 with change in fibre volume fraction V_f. Left figures: elastic properties. Right figures: difference in stiffness between discharged (SOC=0) and charged (SOC=1) state. The fibre volume fraction 0.4 corresponds to the baseline.

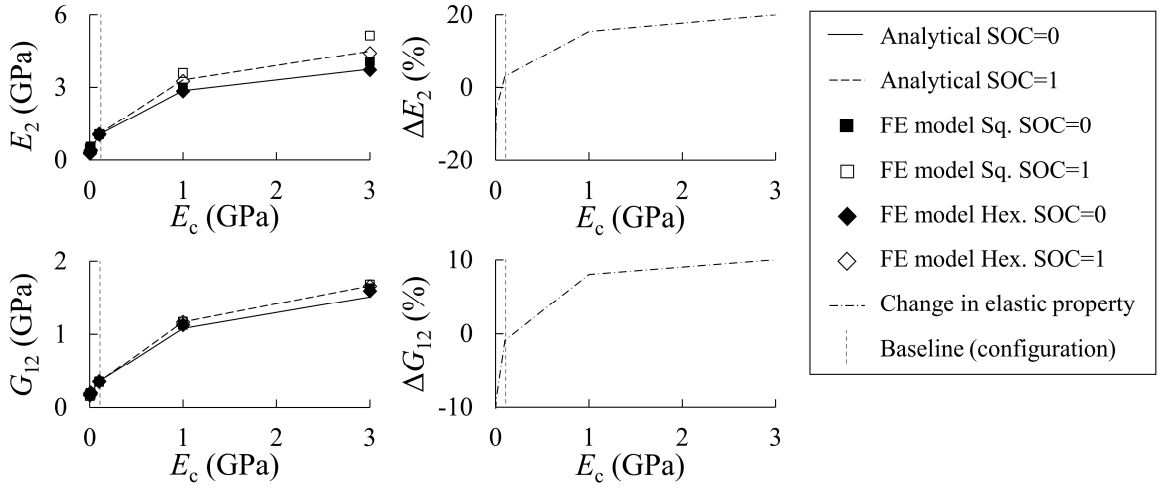

Fig. 5. Variation of effective elastic properties E_2 and G_{12} of the composite lamina at SOC=0 and SOC=1 with change in Young's modulus of coating E_c. Left figures: elastic properties. Right figures: difference in stiffness between discharged (SOC=0) and charged (SOC=1) state. Young's modulus of 0.1 GPa corresponds to the baseline.

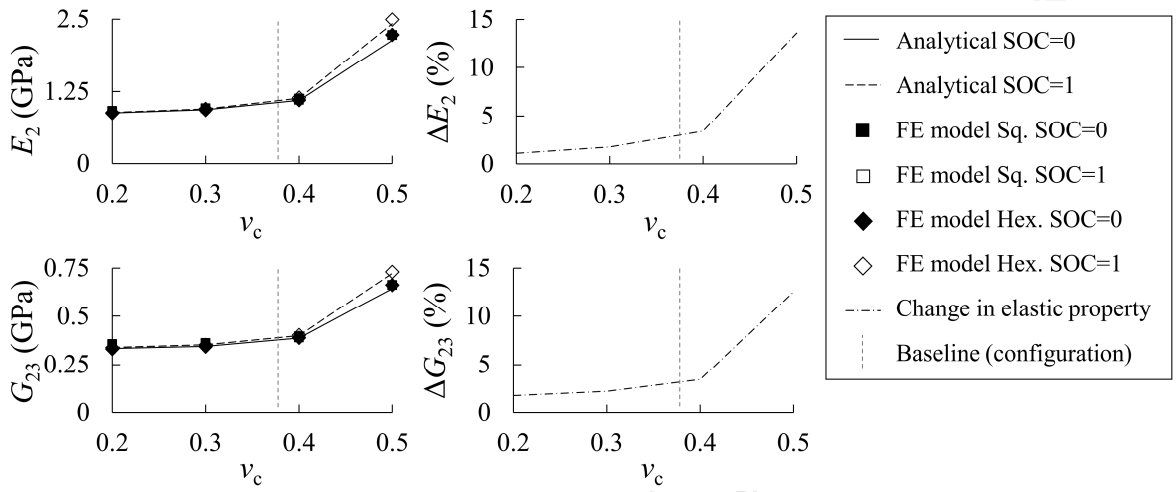

Fig. 6. Variation of effective elastic properties E_2 and G_{23} of the composite lamina at SOC=0 and SOC=1 with change in Poisson's ratio of coating v_c. Left figures: elastic properties. Right figures: difference in stiffness between discharged (SOC=0) and charged (SOC=1) state. Poisson's ratio of 0.38 corresponds to the baseline.

Tables

Table 1. Volume and stiffness changes of the battery electrode materials. The changes are defined as the change moving from the delithiated to the lithiated state of the material.

Electrode material Delithiated	Lithiated	Volume change ΔV (%)	Stiffness changes ΔE^{L} (%)	ΔE^{T} (%)	Reference
$FePO_4$	$LiFePO_4$	5	0	0	[9, 12]
Mn_2O_4	$LiMn_2O_4$	6.8	0	0	[9]
CoO_2	$LiCoO_2$	2	350	350	[9]
Carbon fibre (C)	-	10 (radial dir.)	$-100\left(1-\frac{V_{\mathrm{f},dl}}{V_{\mathrm{f},l}}\right)$	150	[8, 10, 11]

Table 2. Material and geometric properties used as baseline values and range studied in the parametric study.

Material/geometric property	Variable	Baseline value	Range studied		Reference
Fibre volume fraction (-)	V_f	0.4	0.2 – 0.6		
Longitudinal fibre stiffness (GPa)	$E_{\mathrm{f},dl}^{\mathrm{L}}$	290	-		[5]
Transverse fibre stiffness (GPa)	$E_{\mathrm{f},dl}^{\mathrm{T}}$	10	10 – 25		[29]
Change in transverse fibre stiffness with change in SOC (%)	$\Delta E_\mathrm{f}^{\mathrm{T}}$	150	0 – 150		[10, 11]
Shear modulus fibre (GPa)	$G_\mathrm{f}^{\mathrm{LT}}$	10	-		
In-plane and transverse Poisson's ratio fibre (-)	$v_\mathrm{f}^{\mathrm{LT}}$, $v_\mathrm{f}^{\mathrm{TT}}$	0.2	-		
Radius of carbon fibre (µm)	r_f	2.5	-		
E-modulus coating (GPa)	E_c	0.1	0.001 – 3		[6, 28]
Poisson's ratio coating	v_c	0.38	0.2 – 0.49		
Thickness coating (µm)	t_c	0.5	0.2 – 1		[6]
E-modulus matrix excl. particles (GPa)	E_m	0.5	0.001 – 3		[25]
Poisson's ratio matrix (-)	v_m	0.38	-		
Volume fraction of particles within the matrix (-)	V_p^*	0.5	0.2 – 0.6		
Active positive electrode material (-)	-	$FePO_4$	Mn_2O_4	CoO_2	[9, 12]
E-modulus particles (GPa)	$E_{\mathrm{p},dl}$	125	192	60	[9, 12]
Poisson's ratio particles (-)	v_p	0.28	0.24	0.32	[9, 12]

Table 3. The effective elastic properties for the baseline configuration calculated using the analytical model. The results from the FE models are added for validation purpose.

Model	SOC (-)	E_1 (GPa)	E_2 (GPa)	G_{12} (GPa)	G_{23} (GPa)
Analytical	0	116.8	1.052	0.354	0.375
Analytical	1	116.7	1.084	0.351	0.387
Difference (Analytical)	-	-0.1%	3.0%	-0.9%	3.1%
FE model Sq.	0	116.8	1.059	0.351	0.381
FE model Sq.	1	116.7	1.073	0.346	0.383
FE model Hex.	0	116.8	1.048	0.355	0.374
FE model Hex.	1	116.7	1.081	0.350	0.386